Wind and Structures, *Vol. 19, No. 2 (2014) 199-217*
DOI: http://dx.doi.org/10.12989/was.2014.19.2.199

Analysis of the power augmentation mechanisms of diffuser shrouded micro wind turbine with computational fluid dynamics simulations

Seyed A Jafari* and Buyung Kosasih

School of Mechanical, Materials and Mechatronic Engineering, University of Wollongong, Wollongong, NSW 2500, Australia

(Received June 21, 2013, Revised June 23, 2014, Accepted July 6, 2014)

Abstract. Reported experimental and computational fluid dynamic (CFD) studies have demonstrated significant power augmentation of diffuser shrouded horizontal axis micro wind turbine compared to bare turbine. These studies also found the degree of the augmentation is strongly dependent on the shape and geometry of the diffuser such as the length and the expansion angle. However the study of flow field over the rotor blades in shrouded turbine has not received much attention. In this paper, CFD simulations of an experimental diffuser shrouded micro wind turbine have been carried out with the aim to understand the mechanisms underpinning the power augmentation phenomenon. The simulations provide insight of the flow field over the blades of bare wind turbine and of shrouded one elucidating the augmentation mechanisms. From the analysis, sub-atmospheric back pressure leading to velocity augmentation at the inlet of diffuser and lowering of the static pressure on the blade suction sides have been identified as the dominant mechanisms driving the power augmentation. And effective augmentation was achieved for λ above certain value. For the case turbine it is λ greater than ≈ 2.

Keywords: coefficient of performance; computational fluid dynamics; diffuser shroud; micro horizontal axis wind turbine

1. Introduction

Horizontal axis micro wind turbines are potential small scale wind turbines as domestic on-site power generation system in urban built-environment. Micro wind turbines can be used as single system or as part of hybrid system along with photovoltaic system. Micro wind turbines based domestic power generation is new technology with many challenges including high cost to return ratio and low power generation. The main technical challenges concern with (1) continuously changing wind direction; (2) low wind velocity; and (3) high turbulence wind which are very site specific. The take up of micro-wind turbine based power generation may be stimulated if the device can be made to tolerate and produce power in the difficult built-environment wind conditions and support alternative utilization of the technology, for example as power source of

*Corresponding author, Mr., E-mail: sahj551@uow.edu.au

http://www.techno-press.org/?journal=was&subpage=8 ISSN: 1226-6116 (Print), 1598-6225 (Online)

rechargeable devices, domestic sensor/automation smart technology, power for low energy consuming devices in urban environment.

Placing horizontal axis wind turbine in diffuser shroud has been shown to increase the power output compared to a bare turbine. Early experimental studies by Lilley and Rainbird (1956), Foreman *et al*. (1978) and Igra (1981) have demonstrated improved power output of diffuser shrouded wind turbine (*DWT*). A prototype of *DWT* with 3m diameter in $5ms^{-1}$ wind speed was shown to yield power augmentation of two. In all experiments, increased mass flow rate through the rotor were shown to be the primary mechanism of the power augmentation. Igra (1981) further showed that if the diffuser has aerofoil cross section with inverted suction side more air is drawn into the diffuser. The amount of drawn air is limited by separation in the boundary layer along the diffuser wall and the resistance posed by the turbine. As the flow inside a diffuser is subject to adverse pressure gradient, Igra (1981) introduced flaps and slots to energize the boundary layer. Using similar concept, Phillips *et al*. (2002) developed the Vortec 7 *DWT* where multi-slotted diffuser to prevent separation was used.

The relative increase of mass flow rate through the rotor in *DWT* is shown to decrease with increased thrust coefficient by Hansen *et al*. (2000) suggesting that the augmentation is limited to the relative speed-up under zero thrust. Based on inviscid 1D analysis of pressure variation through the duct, Igra (1981) and Lawn (2003) showed that the speed-up is not only influenced by the thrust coefficient but by three other coefficients namely i) shroud inlet efficiency, ii) pressure recovery coefficient, and iii) base pressure coefficient, all of which can be related to the shroud shape and geometry. Van Bussel (2007) showed power augmentation is directly related to mass flow augmentation which is achieved by increasing the exit area ratio and decreasing the back pressure (base pressure coefficient).

To find the influence of shroud geometrical features, Shives and Crawford (2010) using computational fluid dynamics investigated the effect of diffuser with aerofoil (NACA 0015) cross section geometrical features. It was found that inlet efficiency (i) has only small impact on the power output. And flow separation in the diffuser leads to significant lowering of the pressure recovery coefficient (ii) which in turn reduces the overall power coefficient, C_p. Base pressure coefficient (iii) is the most influential parameter in C_p. Base pressure is shown to vary with the diffuser outlet angle and the expansion ratio.

Abe and Ohya (2008) using CFD investigated the effect of adding flange at the diffuser exit plane. The rotor is simulated as loading disk. Disk loading significantly affects the separation in the diffuser hence the pressure coefficient. Ohya *et al*. (2008) showed that with the addition of broad ring flange (*brim*) in the outlet of the diffuser the base pressure at the exit plane can be lowered further due to the vortex formation at the outlet plane. So if compared to same diffuser without brim i.e., both diffuser has the same pressure recovery coefficient, with lower base pressure the flow must expand from lower downstream rotor plane pressure. As the expansion in the brimmed diffuser and non-brimmed one is the same the pressure downstream of the brimmed diffuser turbine must be lower and hence flow greater flow rate is drawn into the rotor (Abe and Ohya 2004). Therefore performance of brimmed diffuser shrouded turbine is greater compared to diffuser only. Chen *et al*. (2012) studied the effect of solidity and wind speed on brimmed diffuser. For the tested DAWT it was found that solidity affects the degree of the augmentation from a diffuser diffuser. An optimum augmentation was seen for rotor with 30%-40% solidity. Beyond this the effect of diffuser diminishes. It was also found that the higher the wind speed the smaller the diffuser's effect is.

Despite of the numerous study of *DWT*, there is little study of the flow over the rotor blade in diffuser shrouded turbine and how it affects the overall performance of *DWT*. This paper therefore focused on simulating micro wind turbine in both bare and diffuser augmented configurations. The simulation results were compared with experimental data achieved in laboratory. The study aimed to explain the power augmentation mechanism from the addition of diffuser.

2. Experimental set-up

A micro wind turbine model has been made in laboratory. This model has three blades and a cylindrical hub. The rig was designed with detachable diffuser allowing comparison of bare turbine against different shrouded turbine geometries with minimum variations other than replacing the diffuser attachment. Fig. 1 show the turbine with no diffuser attached (a) and (b) with diffuser. The model turbine has three blades. The blades have NACA 63-210 airfoil profile. The rotor diameter is 190 mm. The tip gap is kept as small as practically possible i.e., 2-3 mm. The diffuser length is 120 mm resulting in *L/D* of 0.63. The expansion angle α of the diffuser is 12^o which gives diffuser outlet and inlet area ratio of 1.61. The major dimensions of the ducted wind turbine model are given in Table 1. The turbine was placed in a wind tunnel with working section of 450 mm x 450 mm x 1500 mm and wind speed up to $25ms^{-1}$.

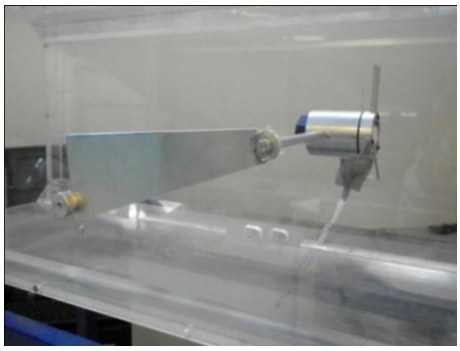

(a)

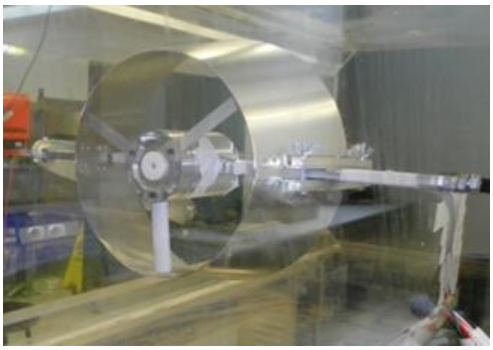

(b)

Fig. 1 Wind Turbine mounted in wind tunnel test section (a) bare turbine and (b) diffuser -augmented turbine

Table 1 Major dimensions of the shrouded wind turbine model

	Dimension	Value	Units
Diffuser	Rotor diameter (*D*)	190	mm
	Outlet diameter	242	mm
	Length (*L*)	120	mm
	Expansion angle ( )	12	degrees
Hub	Diameter	60	mm
	Length	95	mm
Blade	Span	65	mm
	Chord	25	mm
	Thickness	2.5	mm
	Number	3	
	Pitch angle	25	degrees

The wind energy conversion into mechanical power was directly measured from the torque and rpm measurement. In this case, the torque measured is the torque applied directly to the motor stator. The reaction forces that oppose the electromagnetic torque create an equal and opposite torque that is applied to the stator. The turbine is attached to a DC 120 Watt Maxon motor with matching motor controller (4-q-EC Servo amplifier DES70/10). The rotational speed of the rotor can be precisely controlled. As the wind flow over the blades the induced lift produces torque that turns the stator. The free stream wind through the test tunnel section is measured and monitored by an anemometer that feeds into the center of the tunnel section so by controlling the motor speed the motor is acting as brake and the braking torque was measured by the load cell. The rpm of the rotor was then controlled but must be below 2500 rpm. Thus the variation of λ is achieved by varying rpm at the chosen wind speeds.

The experimental procedure was as follows the wind speed to induce 2500 rpm free spinning of the rotor was initially determined. It was found that $10ms^{-1}$ and $7ms^{-1}$ were the required wind speed to spin the rotor at 2500 rpm under no load other than motor resistive load for bare turbine and DAWT respectively. Once these wind speeds had been found, the speed was maintained constant. The rpm of the rotor was then controlled but must be below 2500 rpm. Thus the variation of λ was achieved by varying rpm at the chosen wind speeds.

$$\lambda = \frac{R\omega}{V} \tag{1}$$

The power captured by the turbine is given by the torque measured by the load cell multiplied by the rotor rpm registered by the controller from which C_p is calculated

$$C_p = \frac{P_{measured}}{P_{wind}} = \frac{T\,\omega}{0.5\,\rho\,AU^3} \tag{2}$$

In the case of bare turbine A is the turbine swept area whilst in the case of diffuser augmented turbine A is the diffuser outlet area.

3. Description of the CFD simulations

3.1 Transition - turbulence model

As the flow of over the rotor blades can be subject to significant region of laminar-turbulence transition and because the transition process can affect the separation behavior of the boundary layer on the blade surface, transition SST model (Menter *et al*. 2006) has been used in this work. This model is a modified SST *k-ω* RANS turbulence model by the addition of two other transport equations for the intermittency, γ and the transition onset criteria. The transport equation for the intermittency γ is defined as

$$\frac{\partial(\rho\gamma)}{\partial t}+\frac{\partial(\rho U_j\gamma)}{\partial x_j}=P_{\gamma 1}-E_{\gamma 1}+P_{\gamma 2}-E_{\gamma 2}+\frac{\partial}{\partial x_j}\left[\left(\mu+\frac{\mu_t}{\sigma_y}\right)\frac{\partial\gamma}{\partial x_j}\right] \tag{3}$$

and the second transport equation for the transport of the transition momentum thickness Reynolds number, $\tilde{\mathrm{Re}}_{\theta t}$ is

$$\frac{\partial(\rho\tilde{\mathrm{Re}}_{\theta t})}{\partial t}+\frac{\partial(\rho U_j\tilde{\mathrm{Re}}_{\theta t})}{\partial x_j}=P_{\theta t}+\frac{\partial}{\partial x_j}\left[\sigma_{\theta t}(\mu+\mu_t)\frac{\partial\tilde{\mathrm{Re}}_{\theta t}}{\partial x_j}\right] \tag{4}$$

These equations are coupled with the SST turbulence model

$$\frac{\partial}{\partial t}(\rho k)+\frac{\partial}{\partial x_j}(\rho u_j k)=\tilde{P}_k-\tilde{D}_k+\frac{\partial}{\partial x_j}\left[(\mu+\sigma_k\mu_t)\frac{\partial k}{\partial x_j}\right] \tag{5}$$

$$\frac{\partial}{\partial t}(\rho\omega)+\frac{\partial}{\partial x_j}(\rho u_j\omega)=\alpha\frac{P_k}{\nu_t}-D_\omega+C\,d_\omega+\frac{\partial}{\partial x_j}\left[(\mu+\sigma_k\mu_t)\frac{\partial\omega}{\partial x_j}\right] \tag{6}$$

$$P_k=\gamma_{eff}P_k \tag{7}$$

$$\tilde{D}_k=\min[\max(\gamma_{eff},0.1),1.0]D_k \tag{8}$$

P_k and D_k are the turbulent kinetic energy production and destruction terms in the original SST turbulence model and γ_{eff} is the effective intermittency calculated by the additional two equations.

3.2 Mesh and boundary conditions

The model of the diffuser shrouded turbine is shown in Fig. 2. The volume of fluid was extracted and meshed in Gambit. In order to balance between solution accuracy and calculation time, a combination of structured and unstructured mesh was used. Although structured mesh was the preferred method for wind turbine analysis it is difficult to generate a high quality structured mesh throughout the volume so the duct was divided into two parts i.e., (i) one disk including the rotor and (ii) the rest of the duct except this disk. Unstructured mesh was used around the rotor surface within the disk and structured mesh was used in the rest of the duct. These two parts are shown in Fig. 3 showing fine tetrahedral grids on the rotor surface. This technique aims at

generating a high quality mesh for the investigation of the flow mechanism in close and far regions from the rotor. The final mesh consists of 1,102,654 cells with 568,142 hexahedral cells (structured grids), and 534,532 pyramidal and tetragonal cells (unstructured grids).

To model the dynamic geometry such as wind turbine, Multiple Reference Frame (*MRF*) methodology is used. *MRF* is a steady-state approximation in which individual cell zones is assigned different rotational and/or translational speeds. In MRF, two reference frames: (i) a stationary frame relative to the diffuser walls; and (ii) rotating frame simulating the rotating turbine are used. In the stationary domain flow properties are solved in the stationary reference frame whilst in the rotating domain they are solved in rotating frame.

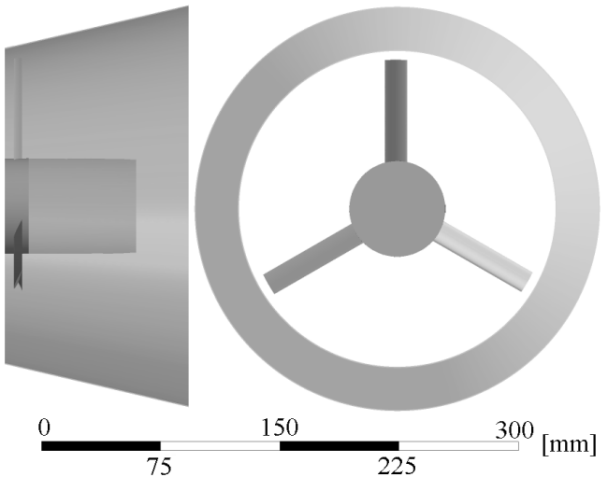

Fig. 2 Front and side view of MWT rotor and diffuser developed for the CFD simulations

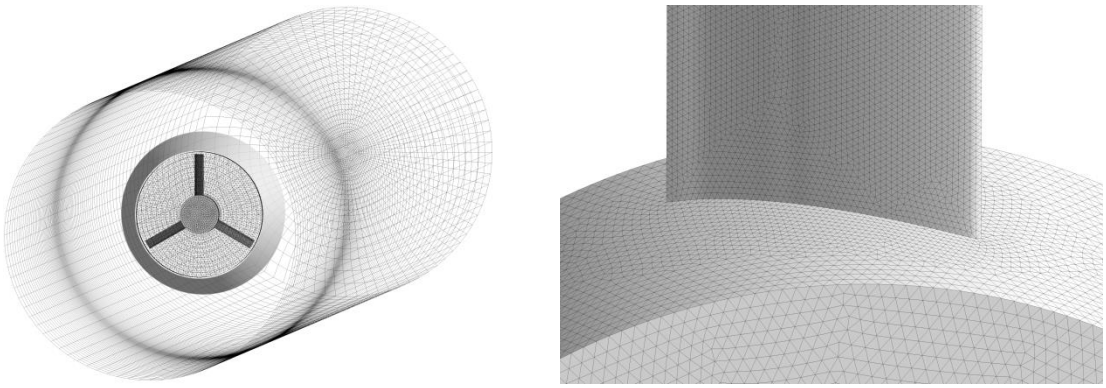

(a) (b)

Fig. 3 (a) overview of the mesh of the simulation domain and (b) fine tetrahedral grids used on blade

The quadrangular wind tunnel in the experimental test is replaced by a circular duct with same length and 500 mm diameter in the CFD model. The symmetry of the circular duct allows doing the simulation in only one third of the entire geometry and assists to reduce the solution time. A solid blockage effect is commonly observed in wind tunnel testing which creates an increase in the local wind velocity in the working section. This increase is accounted for by a theoretical wind tunnel blockage ratio. The blockage ratio is the percentage of the test section that is blocked by the model. Diameter of the circular duct in the CFD model is selected so that makes a cross section area equal to the experimental wind tunnel. This results in an equal blockage ratio in both models and minimizes the deviation of the flow velocity when passing the MWT in the CFD model from when in the experimental model.

Inlet boundary condition is constant free stream velocity of $5ms^{-1}$ whilst the outlet boundary of the domain was set to atmospheric pressure. In low-turbulence wind tunnels, the free-stream turbulence intensity is low, hence turbulence intensity of 0.1% and turbulence viscosity ratio of 1 were set for both inlet and outlet boundary conditions. The standard pressure correction method and a first order upwind scheme was used. The sides' walls were set as stationary wall with no-slip boundaries. The duct and the diffuser were set as moving walls with absolute rotational velocity of zero while the rotor blades and the hub were set as wall attached to moving frame. In order to measure Cp for various conditions, rotational speed of the MRF was changed from 0 rpm ($\lambda = 0$) to 2000rpm ($\lambda = 4.5$) with increment of 250 rpm ($\lambda = 0.5$).

4. Results and discussion

4.1 Coefficient of performance, C_p and coefficient of thrust, C_T

A comparison between C_p and C_T of the MWT and DAMWT is shown in Fig. 4 to assess the effect of diffuser on the power output. As can be seen the maximum C_p of the MWT obtained by CFD simulation is 13.8% achieved in λ= 2.3 while in the DAMWT it is 19.5% and in λ = 3, which means the performance has 41.3% increased. This indicates that at low λ, MWT and DAMWT C_p curves agree well, but at higher λ power extraction increases by increasing λ until an optimum point, at which further increase in λ reduces C_p.

The figure shows for λ< 2 adding diffuser does not improve the performance of the turbine in term of C_p. This indicates that at higher wind speed (lower tip speed ratio) the effect of diffuser is diminished. Physically this may be explained as follow. As more air mass is drawn into the diffuser the rotor needs to spin at higher rpm to capture the wind kinetic energy. For the same rpm the angle of attack of the inlet air for the DAMWT is higher than the MWT resulting in lower lift due to stall angle. As a result C_p of the DAMWT is lower than the MWT in lower λ .

The λ at which the effect of diffuser is noticeable shown in the experimental curves is $\lambda \approx 1.5$. This is qualitatively agreed well with the simulation result value of $\lambda \approx 2$. Ohya and Karasudani (2010) showed similar phenomenon for shrouded wind turbine with wind-lens technology. Additionally Chen *et al*. (2012) found that the effect of flanged diffuser is felt less in higher wind speed. It is conclusive that diffuser shrouded micro wind turbine will need to operate at much higher rpm (higher tip speed ratio) than bare wind turbine for it to be beneficial. Because of this the rotor generator matching must be designed accordingly.

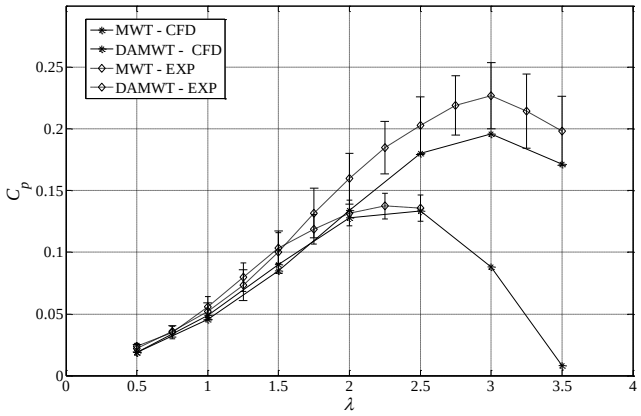

Fig. 4 Comparison of C_p of MWT and DAMWT against λ

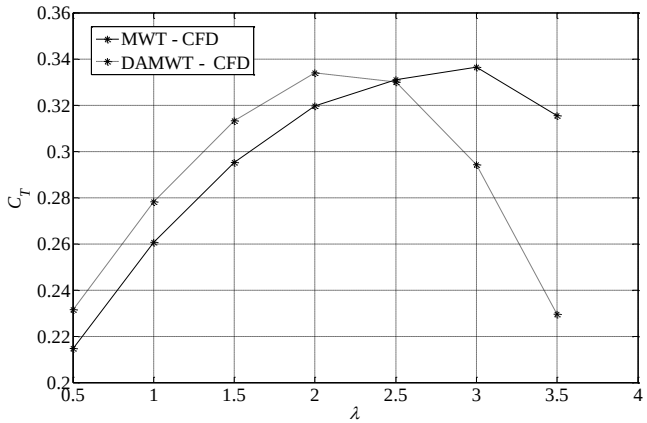

Fig. 5 Comparison of CT of MWT and DAMWT against λ

Other point to note from Fig. 4 is that both the experiment and the simulation results demonstrate significant power augmentation due to diffuser effect in higher λ. The power augmentation of the experiment is seen more than the simulation. There are few reasons that can affect the difference e.g., greater turbulent intensity of the free stream wind and the fluctuating wind speed during the experiment which we could not eliminate.

Effect of diffuser over C_T was also investigated. C_T is given by the definition

$$C_T = \frac{F_{axial}}{0.5\rho A\, U^2} \tag{9}$$

Fig. 5 shows C_T obtained by CFD simulations for the MWT and DAMWT. Maximum C_T is 33.3% in MWT and 33.8% in DAMWT. Further increase in λ serves to reduce amount of thrust

force exerted on the rotor. The maximum C_T was obtained at λ = 2 in MWT while for DAMWT it has shifted to λ= 3. This is very close to what was seen in C_p augmentation. However maximum C_T has increased only 8%, which is much lower than C_p augmentation. This shows that although increase in thrust force leads to higher power augmentation, this is not the only factor which affects this augmentation, and operating in higher rpm may have a greater impact on power augmentation.

4.2 Velocity augmentation

With no turbine within the diffuser and by neglecting the heat transfer and friction in the diffuser, the flow could be considered as isentropic flow. In this situation the average velocity at the rotor plane would increase from 5ms^{-1} to 7.888ms^{-1} which represents 57.6% augmentation. Fig. 6 show velocity contour of the air passing the turbine rotor in λ = 3.5. The average velocity of the air passing the rotor plane has increased around 32% with diffuser which is much smaller than 57.6%. As rpm is lower the velocity augmentation is closer to 57.6%. For λ = 2 average velocity of the air passing the rotor area has increased around 37%. This demonstrates that the degree of mass flow augmentation is also affected by increase in the rotor rpm.

Fig. 6 shows the non-uniform induced velocity across the rotor in λ =3.5, where the greatest augmentation contribution appears mainly from the tip region. This velocity augmentation is created by flow expansion which is because of the pressure reduction at the outlet of the diffuser. Figs. 7 to 9 depict the relative static pressure at the diffuser outlet. The pressure behind the bare turbine is recovered quickly to the atmospheric value but at the outlet of the diffuser is still much lower than atmospheric pressure. It should be noted that the pressure is not uniform. At low λ (low rpm or high wind speed) instantaneous lowest pressure seem to be following the blade while at higher λ (=2 and 3.5) the pressure is stratified with the lowest at the core.

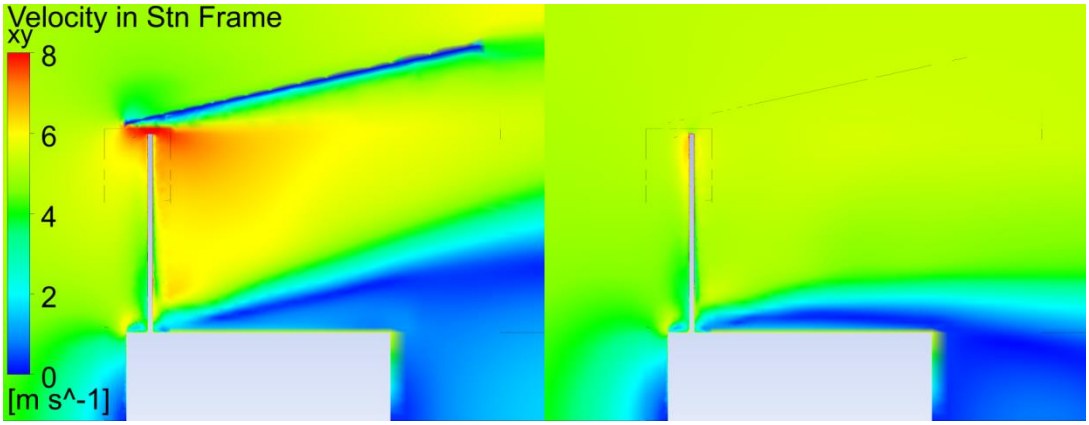

(a) (b)

Fig. 6 Distribution of velocity in (a) DAMWT and (b) MWT in λ =3.5

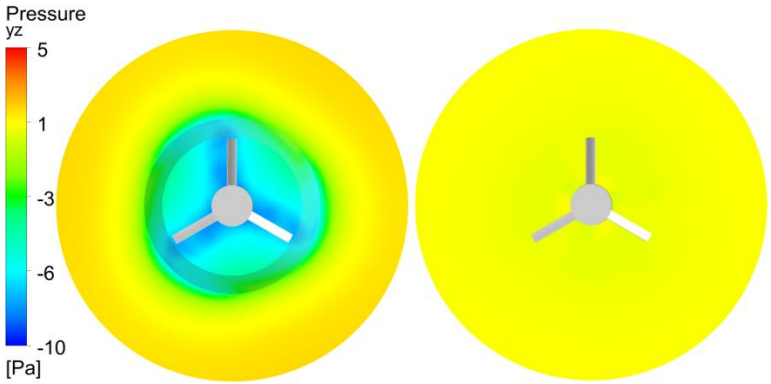

Fig. 7 Pressure distribution at the outlet of diffuser in MWT (right) and DAMWT (left) in λ =0.5

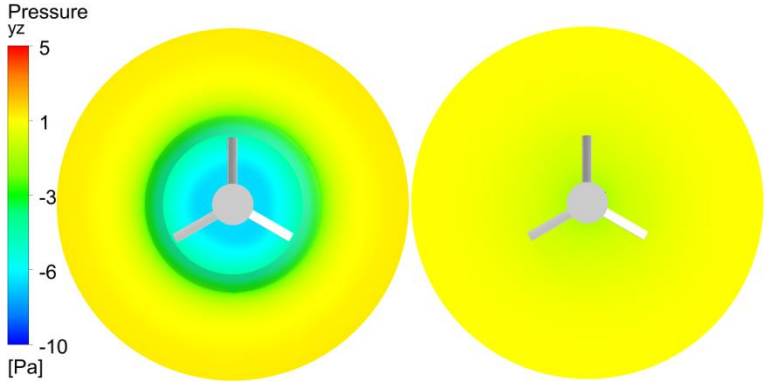

Fig. 8 Pressure distribution at the outlet of diffuser in MWT (right) and DAMWT (left) in λ =2

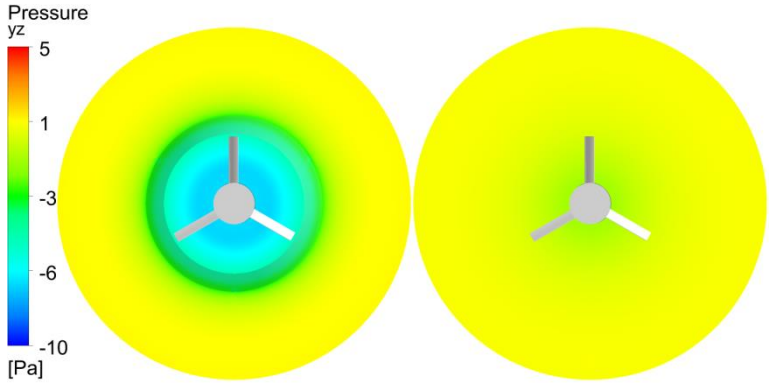

Fig. 9 Pressure distribution at the outlet of diffuser in MWT (right) and DAMWT (left) in λ =3.5

4.3 Blade surface pressures

The pressure on the blade surface provides torque to turn the rotor and convert the wind kinetic energy to mechanical energy. Whereas the increased mass flow rate increase the power production also by increasing rotor's rotational speed. Lift force on blades is the result of pressure difference between the pressure side and suction side of the blades.

Figs. 10 to 12 compare pressure distribution on pressure side of the MWT and DAMWT blade in λ= 0.5, 2 and 3.5. And Figs. 13 to 15 compare the corresponding pressure distribution on suction side of the MWT and DAMWT blade. As seen in Figs. 13 to 15 pressure values on blades in DAMWT is much less than MWT. From Figs. 10 and 11 for λ = 0.5 - 2 the pressure on pressure side of bare ad shrouded turbine is not much different. When λ = 3.5 both surfaces show negative pressure near the tip. This indicates the location of the inverse lift. However the DAMWT has smaller region of inverse lift which may be attributed to greater axial velocity. This is explained as follow.

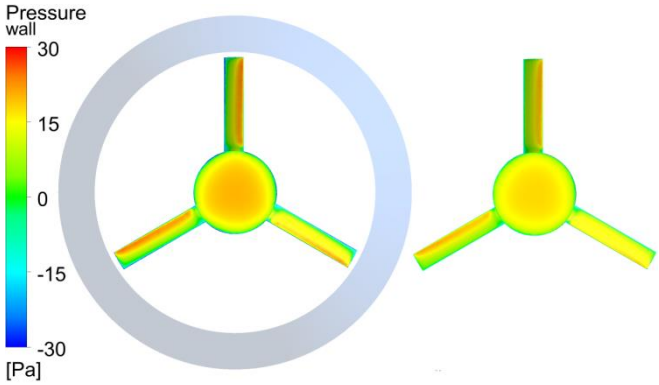

Fig. 10 Pressure distribution on pressure side of the MWT (right) and DAMWT (left) rotor in λ=0.5

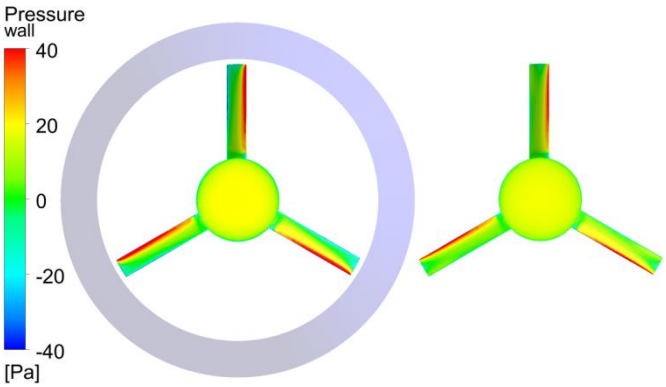

Fig. 11 Pressure distribution on pressure side of the MWT (right) and DAMWT (left) rotor in λ=2

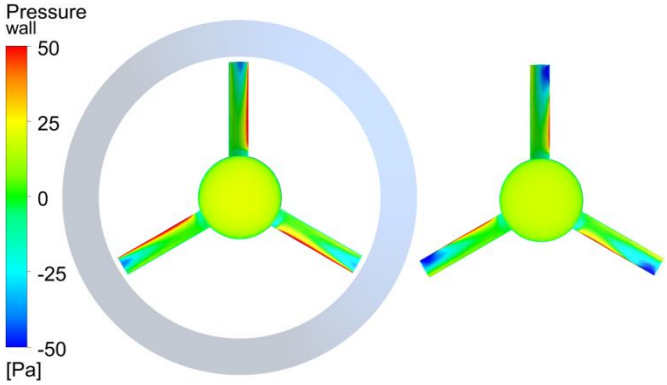

Fig. 12 Pressure distribution on pressure side of the MWT (right) and DAMWT (left) rotor in λ = 3.5

Increase in λ results in higher tangential velocity of the air over the blade and local λ increases from the blade root to its tip. In an untwisted blade (like in this case) as tangential velocity increases, the angle of attack decreases. This decrease may continue to a point, which negative angle of attack exist and at this point inverse lift on blade reducing the total torque. From the analysis it is seen that with diffuser axial velocity increases resulting in increased angle of attack and sustain positive angle of attack and lift. It can be concluded that the diffuser influence on surface pressure on the pressure side is seen at higher λ. While the pressures on the suction sides appear to be more affected by the diffuser as demonstrated by Figs. 13 to 15 for all λ, albeit the effect becomes more significant at higher λ.

Figs. 16 to 18 show pressure distribution at different span-wise locations of the blade for λ=0.5, 2 and 3.5. Common feature of the pressure distribution is that the pressure distribution on the pressure side is not affected by the diffuser for all λ. For λ = 0.5, the pressure distribution shape is uniform along the span (Fig. 16). Despite of the seemingly large pressure difference between MWT and DAMWT compared to higher λ (2 and 3.5) the diffuser power augmentation is less significant. This is because the large pressure difference results in higher thrust rather than lift at low λ. This is an explanation why the effect of the diffuser is insignificant at low λ (see Fig. 4).

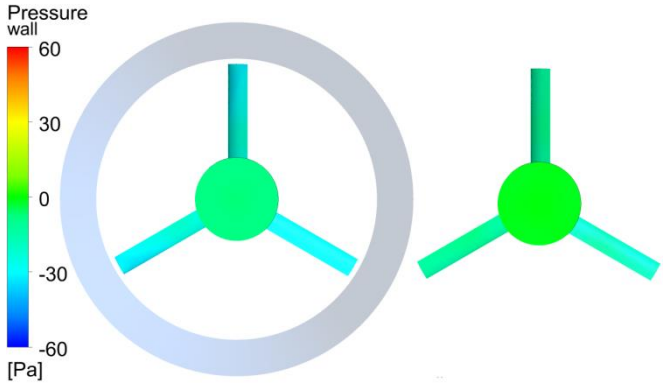

Fig. 13 Pressure distribution on suction side of the MWT (right) and DAMWT (left) rotor in λ = 0.5

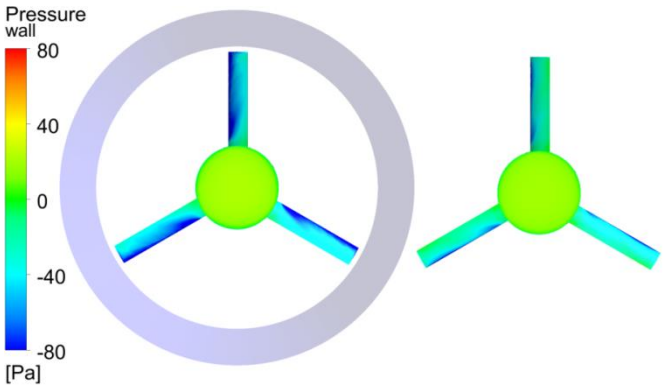

Fig. 14 Pressure distribution on suction side of the MWT (right) and DAMWT (left) rotor in λ = 2

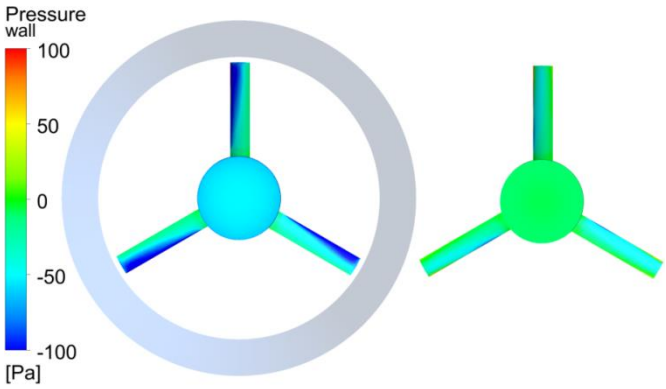

Fig. 15 Pressure distribution on suction side of the MWT (right) and DAMWT (left) rotor in λ = 3.5

When λ is 2 the pressure distribution is no longer uniform along the span. The distributions on the pressure and suction sides change along the span which may be induced by the radial flow component. Toward the tip the contribution from the leading edge becomes more dominant. It appears for MWT the contribution of the outboard region diminishes whilst with DAMWT significant pressure difference still exists.

Pressure distributions on both sides of the blade vary along the blade span as well as along the chord of the blade when λ = 3.5. This indicates the coupled effect of the radial flow component and the diffuser. The contribution of the outboard section r/R = 0.973 is almost diminished in MWT while the DAMWT continue to have pressure difference.

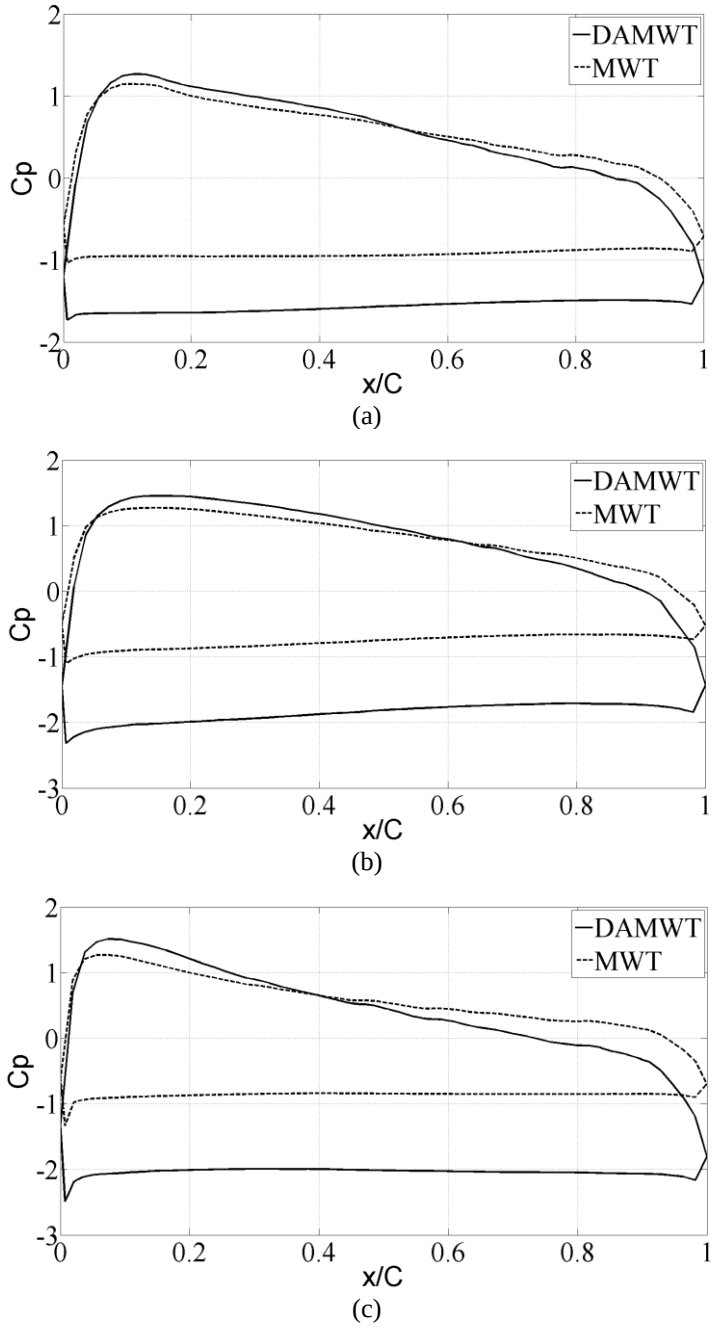

Fig. 16 Pressure magnitude on the MWT and DAMWT blade in λ =0.5 at (a) r/R=0.342, (b) r/R=0.658 and (c) r/R=0.973. Note x/C = 0 corresponds to the leading edge and x/C = 1 to the trailing edge

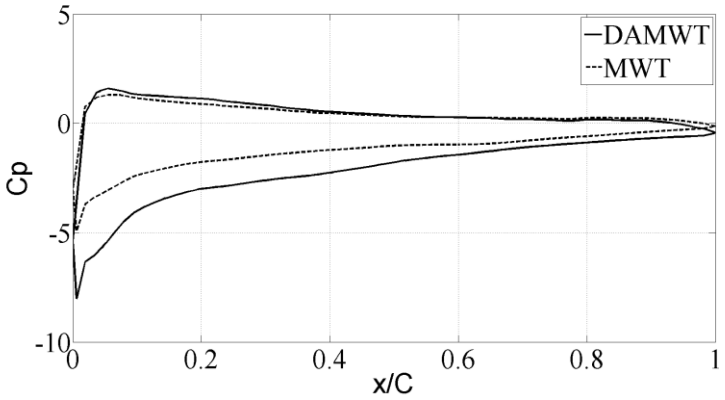

(a)

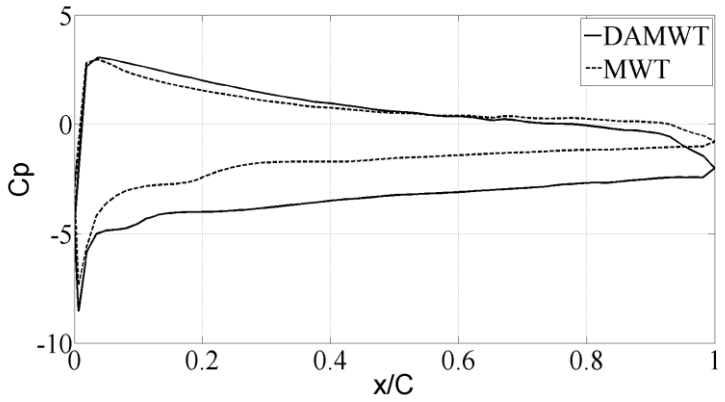

(b)

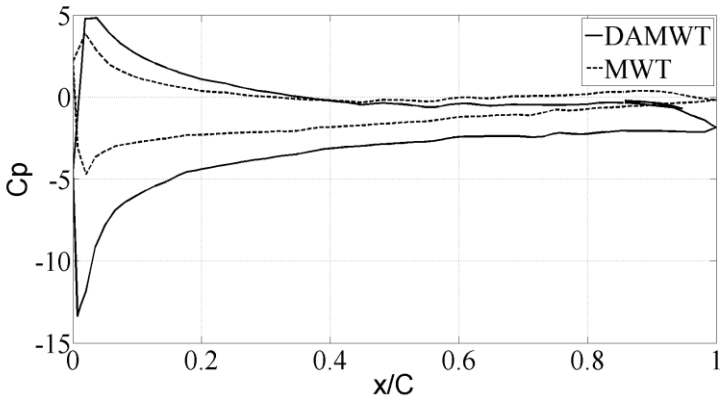

(c)

Fig. 17 Pressure magnitude on the MWT and DAMWT blade in $\lambda = 2$ (a) r/R=0.342, (b) r/R=0.658 and (c) r/R=0.973. Note x/C = 0 corresponds to the leading edge and x/C = 1 to the trailing edge

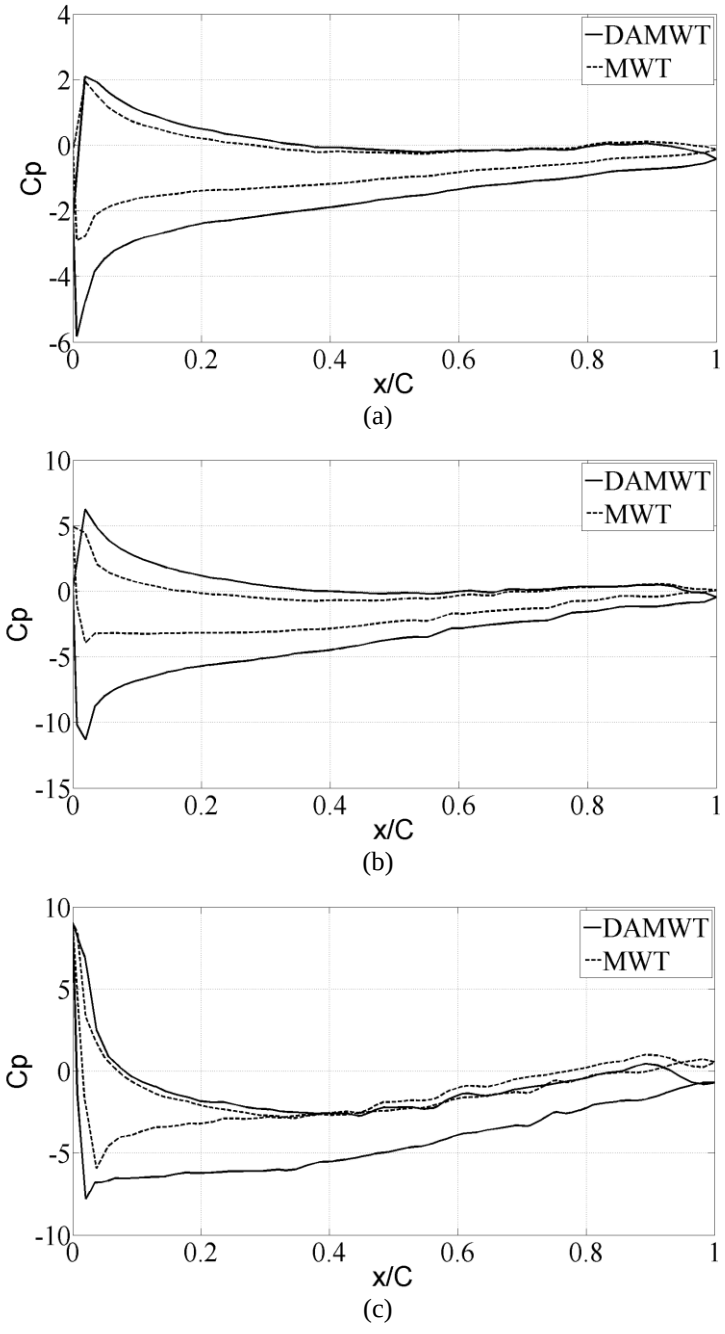

Fig. 18 Pressure magnitude on the MWT and DAMWT blade in $\lambda = 3.5$ (a) r/R = 0.342, (b) r/R = 0.658 and (c) r/R = 0.973. Note x/C = 0 corresponds to the leading edge and x/C = 1 to the trailing edge

5. Conclusions

CFD analysis of bare (MWT) and diffuser shrouded (DAMWT) turbine of the same rotor was performed in this study. The Simulations were first compared with experimental result in term of the turbine power coefficient. The analysis demonstrates the difference in performance characteristics of bare and diffuser shrouded turbine and sheds insight of the power augmentation mechanisms. Qualitatively power augmentation of a diffuser appears only above a certain value of tip speed ratio. The augmentation is not solely the result of mass flow rate increase but also the change of pressure distribution on the blade surfaces affected by the diffuser. In general diffuser shrouded need to operate at higher rpm and because of this the generator and rotor matching for this kind of turbine must take into account this feature.

Acknowledgments

The computing resource used in this work and the experimental rig expenses were supported by 2012 University of Wollongong URC grant.

References

Abe, K. and Ohya, Y. (2008), "An investigation of flow fields around flanged diffusers using CFD", *J. Wind Eng. and Ind. Aerod.*, **94**, 315-330.

Chen, T.Y., Liao, Y.T. and Cheng, C.C. (2012), "Development of small wind turbines for moving vehicles: effects of flanged diffusers on rotor performance", *Expert. Thermal Fluid Sci*., **42**, 136-142.

Digraskar, D.A. (2010), *Simulations of flow over wind turbines*, Master Thesis, University of Massachusetts – Amherst.

Foreman, K.M., Gilbert, B. and Oman, R.A. (1978), "Diffuser augmentation of wind turbines", *Solar Energy*, **20**, 305-311.

Hansen, M.O.L., Sorensen, N.N. and Flay, R.G.J. (2000), "Effect of placing a diffuser around a wind turbine", *Wind Energy*, **3**(4), 207-213.

Igra, O. (1981), "Research and development for shrouded wind turbines", *Energy Conv. Mgmt*., **21**(1), 13-48.

Lawn, C.J. (2003), "Optimization of the power output from ducted wind turbines", *Proc. Instn. Mech. Engrs Part A J. Power Energy*, **217**, 107-117.

Lilley, G.M. and Rainbird, W.J. (1956), A preliminary report on the design and performance of a ducted windmill.

Menter, F.R., Langtry, R.B., Likki, S.R., Suzen, Y.B., Huang, P.G. and Völker, S. (2006), "A correlation-based transition model using local variables – Part I: model formulation", *J. Turbomach*., **128**(3), 413-422.

Ohya, Y., Karasudani, T., Sakurai, A., Abe, K. and Inoue. M. (2008), "Development of a shrouded wind turbine with a flanged diffuser", *J. Wind Eng. Ind. Aerod*., **96**(5), 524-539.

Ohya, Y. and Karasudani, T. (2010), "A shrouded wind turbine generating high output power with wind-lens technology", *Energies*, **3**(4), 634-649.

Phillips, D.G., Richards, P.J. and Flay, R.G.J. (2002), *Diffuser development for a diffuser augmented wind turbine using computational fluid dynamics*.

Shives, M. and Crawford, C. (2010), "Computational analysis of ducted turbine performance", *Proceedings of the 3rd Int. Conf. on Ocean Energy*, 6 Oct. 2010, Bilbao.

Wang, J., Piechna, J. and Muller, N. (2013), "Computational fluid dynamics investigation of a novel multiblade wind turbine in a duct", *J. Solar Energy Eng*., **121**, 011007-011006.
Van Bussel, G.J.W. (2007), "The science of making more torque from wind: diffuser experiments and theory revisited", *J. Phys. Conference Series*, **75**, 1-12.

CC

Nomenclature

A	swept area of the rotor (m^2)
C_p	power coefficient (dimensionless)
C_T	trust coefficient (dimensionless)
D_k	turbulent kinetic energy destruction ($m^2 s^{-2}$)
F_{axial}	thrust force exerted on the rotor (N)
k	turbulent kinetic energy ($m^2 s^{-2}$)
M	Mach number
P	power (W^2)
P_k	turbulent kinetic energy production ($m^2 s^{-2}$)
r	distance to hub center (m)
R	distance from tip of the blade to hub center (m)
$\tilde{\mathrm{R}}e_{\theta t}$	local transition onset momentum thickness Reynolds number
U	velocity of air ($m\ s^{-1}$)
γ	distance to nearest wall (m)
γ_{eff}	effective intermittency (dimensionless)
λ	tip speed ratio (dimensionless)
μ	molecular viscosity (Pa s)
μ_t	eddy viscosity (Pa s)
ρ	air density ($kg\ m^{-3}$)
τ	torque excreted on the rotor
ω	rotational of rotor speed ($rads^{-1}$)